JOURNAL OF ENGINEERING AND APPLIED SCIENCE, VOL. 67, NO. 8, DEC. 2020, PP. 2093-2108
FACULTY OF ENGINEERING, CAIRO UNIVERSITY

SEISMIC DAMAGE BEHAVIOR OF SQUARE STEEL TUBE COLUMN FILLED WITH AEOLIAN SAND CONCRETE

Y. H. WANG[1], Y. P. WANG[2], G. Z. HUO[2], M. ZHAO[2],
J. QI[2], H. Y. WANG[2], AND P. Q. LIU[2]

ABSTRACT

Making full use of the application of Aeolian sand in the steel-concrete composite structure can reduce project costs, save resources, protect the environment, and promote the harmonious development of man and nature. It is necessary to study the seismic behavior and resilience performance of square steel tube columns filled with Aeolian sand concrete. Therefore, in this study, a reversed cyclic load test on a four square steel tube column filled with Aeolian sand concrete was conducted to compare and analyze the failure form, hysteretic behavior, ductility and skeleton curve of each specimen. Then, a three-fold line recovery force model suitable for square steel tube columns filled with Aeolian sand concrete was proposed. Experimental results showed that the setting of the outer square steel tube can improve the brittleness and internal defects of internal concrete, optimize its mechanical properties, and effectively enhance the seismic behavior and post-earthquake recovery performance of specimens. In addition, the proposed theoretical model of the restoring force aligns well with the experimental results, which can be used for the elastic-plastic seismic response analysis of steel–concrete composite structures filled with Aeolian sand.

KEYWORDS: Concrete-filled square steel tubular column, Reversed cyclic loading test, Restoring force model, Aeolian sand concrete.

1. INTRODUCTION

Today, as the world moves towards globalization, urbanization is developing rapidly. While countries are improving infrastructure and speeding up the use of rivers and mountain sands, such excessive utilization greatly threatens the original ecological environment. Therefore, using appropriate amount of Aeolian sand to replace some

[1] Associate Professor, School of Civil Engineering, Inner Mongolia University of Technology, Hohhot, China., wyh@imut.edu.cn
[2] M. Sc. Candidate, School of Civil Engineering, Inner Mongolia University of Technology, Hohhot, China.

traditional engineering sand could contribute to protect the ecological environment and reduce the engineering cost.

Experimental researches on this topic by scholars both in China and abroad [1-3] presented some experimental studies on the compressive strength, freeze-thaw cyclic test and damage model. The results show that replacing river sand with an appropriate amount of Aeolian sand can improve the mechanical properties of the specimens. Wu et al. [4] studied the seismic behavior of steel tube ultra-high-performance concrete short columns. The research results showed that the square steel tube column filled with ultra-high-performance steel fiber concrete demonstrated better ductility, energy consumption and hysteresis behavior than ordinary ones. Several researchers [5-7] used finite element modeling to study the structural performance of rectangular concrete-filled steel tubes, I-section reinforced concrete steel tubes and composite circular concrete-filled steel tubes under torsion and bending. Numerical analysis shows that the proposed design equations for bending, torsion strength and shear of the steel tube composite structural column are safe. Wang et al. [8] investigated the seismic behavior of desert sand concrete columns and common concrete columns through cyclic loading tests. The skeleton curve, hysteretic curve, energy dissipation, ductility, and stiffness of the two kinds of specimens were compared and investigated. The experiment results showed that the energy dissipation capacity of the desert sand concrete columns is higher than the ordinary concrete columns. This result provided a test basis for revealing the seismic mechanism of desert sand concrete columns.

Although many scholars in China and abroad have done a lot of research on the mechanical properties, few people focused on the seismic behavior and the restoring force model of a square steel tube column filled with Aeolian sand concrete. In this study, four square steel tube concrete specimens with different Aeolian sand replacement rates are designed and manufactured. Moreover, the seismic behavior and restoring force model of a square steel tube column filled with Aeolian sand concrete were analyzed through reversed cyclic loading tests.

2. TEST PROGRAM

2.1 Materials

Aggregate consists of extra fine Aeolian sand and natural river sand, with the fineness modulus of natural river sand being 2.7. Coarse aggregate is natural river pebbles with a particle size of 5–25mm and continuous gradation. The sample mix ratio is presented in Table 1. The steel tube adopts a seamless square steel tube with a nominal wall thickness t=3 mm. The basic mechanical properties of the measured steel pipe are shown in Table 2, in which, d, f_y, f_u and E_s represent the diameter, yield strength, tensile strength, and elastic modulus of the steel pipe, respectively. The ratio *A* indicates the elongation of the steel pipe after breaking.

Table 1. Concrete material category and proportion.

Concrete strength	Composition and dosage/kg·m^{-3}					
	Cement	Coal Ash	Water	Stone	Sand+Aeolian Sand	Water Reducing Agent
C40	389.28	43.62	205	1266	492.3	3.27

Table 2. Mechanical properties of rolled steel.

Square steel tube	mark	d, mm	f_y, MPa	f_u, MPa	E_s, MPa	A, %
	Q235	250	340	440	2.20×105	30

2.2 Specimen Design

The data of test specimen ARC1 to ARC4 comes from the paper, which was published by our research group [9]. These data are mainly used for comparative analysis. Wang et al. [9] mainly studied the seismic performance of Aeolian sand concrete columns at different replacement percentage of Aeolian sand. In this paper, a square steel tube column filled with Aeolian sand concrete is designed to be the experimental object. A total of four specimens are designed and produced in this test, with specimen numbers as FARC1 to FARC4. The test pieces FARC1, FARC2, FARC3 and FARC4 are square steel tube columns filled with Aeolian sand based on Aeolian sand replacement rates of 10%, 20%, 30% and 40%, respectively. The dimensions of the test pieces are 250mm × 250mm × 1350 mm, as shown in Fig. 1.

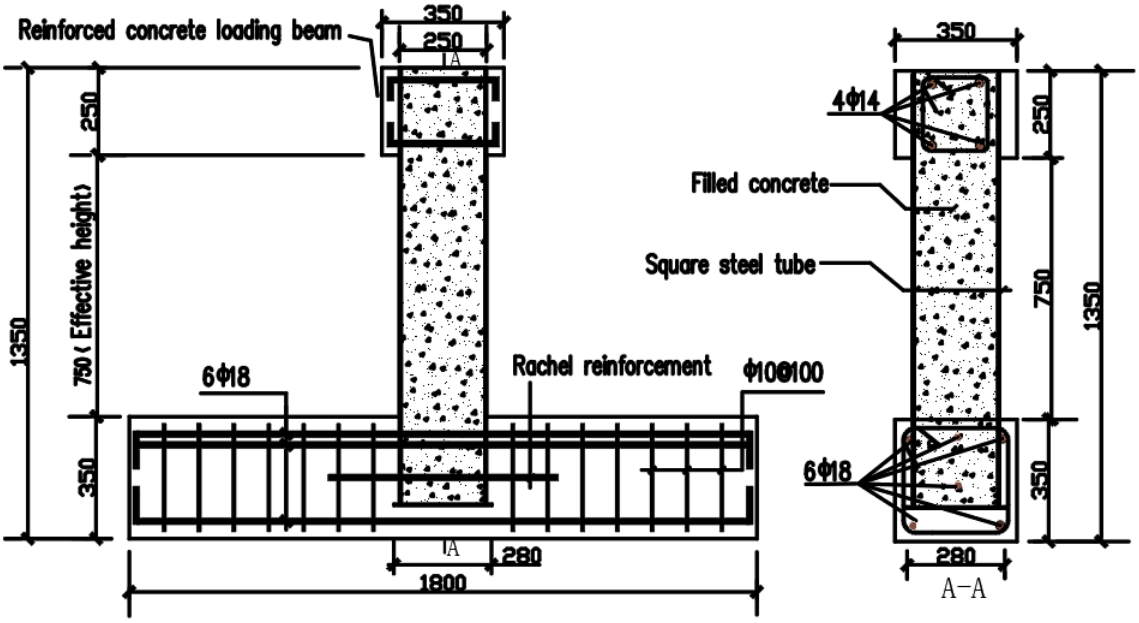

Fig. 1. Design details of the test piece (unit: mm).

The steel tube width-to-thickness ratio is 83.3. The basic parameters of the specimens are listed in Table 3. In the table, f_{cu} is the cubic compressive strength of the concrete column, f_c is the axial compressive strength of the concrete, f_s is the design value of the tensile and compressive strength of the square steel tube, while λ is the index of the specimen ferrule, and $\lambda = A_s f_s/(A_c f_c)$. A_s and A_c represent the cross–sectional area of the steel tube and test piece, respectively. The axial pressure ratio $\eta = N/(A_c f_c)$, with N being the average value of the constant vertical axial force.

Table 3. Specimens parameters.

Specimens	f_{cu}, MPa	f_s, MPa	f_c, MPa	λ	N	η
ARC1	39.1	—	26.2	—	257.1	0.2
ARC2	39.5	—	26.4	—	259.1	0.2
ARC3	40.4	—	27.0	—	264.9	0.2
ARC4	40	—	26.8	—	263.0	0.2
FARC1	39.3	308.0	26.3	0.58	258.1	0.2
FARC2	39.6	308.0	26.5	0.58	260.0	0.2
FARC3	40.2	308.0	26.9	0.57	264.0	0.2
FARC4	40	308.0	26.8	0.57	263.0	0.2

2.3 Specimen Loading

The experiments were conducted at the Key Laboratory of Civil Engineering Structure and Mechanics of the Inner Mongolia University of Technology. The test

device is shown in Fig. 2. The vertical load was applied by a hydraulic jack and the axial pressure remains unchanged. The horizontal load was applied by the electro-hydraulic servo loading system fixed on the reaction wall.

Fig. 2. Test live picture.

A loading method based on force–displacement compound control was adopted in this test. Before the structure entered the plastic yielding stage, the lateral loading was controlled by force. When the square steel tubes yield, the yielding plastic stage was defined, and the displacement control loading was adopted. The experiment was terminated once the horizontal load of the loaded beam dropped to 85% of the peak load or the specimen was significantly damaged.

3. TEST RESULTS AND ANALYSIS

3.1 Hysteresis Performance and Skeleton Curves

The measured hysteresis and skeleton curve of the column specimens are shown in Fig. 3. It can be observed that the hysteresis and skeleton curve are close to a straight line at the initial stage of loading, indicating that the specimens are in the elastic stage, and there is hardly any stiffness degradation or residual deformation. As the cyclic load increases, the slopes of the hysteresis and skeleton curves decrease. The result indicated that the stiffness of the specimens gradually degrades, while the residual deformation increases, which means the specimens enter the elastic–plastic stage. In the late loading period, the hysteretic curve of specimens FARC1 to FARC4 hardly exhibit "shrinkage" phenomenon, and hysteretic curves are full. This indicates

that the FARC1 to FARC4 have better hysteresis performance and energy consumption ability. At the same displacement, the residual deformation of specimen FARC1 to FARC4 are smaller than that of ARC1 to ARC4, which indicates that in the same Aeolian sand and replacement rate, the outer square steel tube can effectively improve the post-seismic recovery performance of the square steel tube columns filled with Aeolian sand concrete.

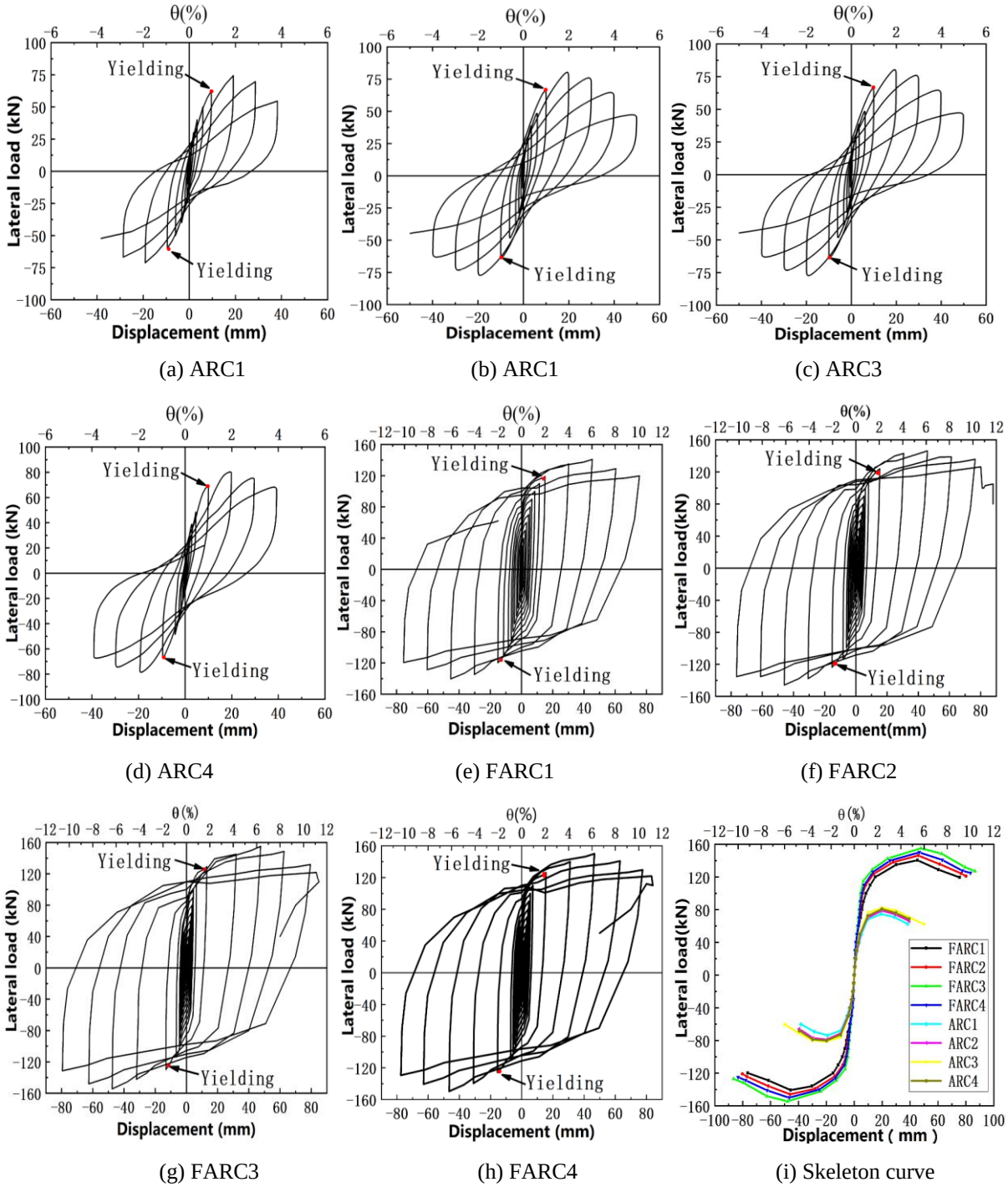

(a) ARC1 (b) ARC1 (c) ARC3

(d) ARC4 (e) FARC1 (f) FARC2

(g) FARC3 (h) FARC4 (i) Skeleton curve

Fig. 3. Hysteresis and skeleton curves of specimens.

3.2 Feature Point Analysis

The characteristic points of each specimen are listed in Table 4, where F_{cr} and Δ_{cr} are the load and corresponding displacement of the specimen cracks, respectively. Similarly, F_y and Δ_y indicate the load and corresponding displacement of the specimen yields. F_m and Δ_m represent the peak load and corresponding displacement of the specimen peaks, respectively. When the lateral load drops to 85% of the peak load, the specimen fails. F_u and Δ_u are defined as the failure load and corresponding displacement of the specimen. The ultimate bearing capacity of test pieces FARC1 to FARC4 are significantly higher than that of ARC1 to ARC4. This is because the square steel tube concrete can combine the two advantages of the high compressive strength of concrete with the strong bending resistance of the square steel tube, which can make the core concrete in a three-way compression state, resulting in a significant increase in the compressive strength of core concrete. Meanwhile, the bearing capacity of specimens FRAC1 to FARC4 is greatly increased. Compared with the test pieces ARC1 to ARC4, the ultimate bearing capacity of the test pieces FARC1 to FARC4 is increased by 84.5%, 85.7%, 88.3% and 86.1%, respectively. It is confirmed that with the same Aeolian sand replacement rate, the outer square steel tube can effectively improve the seismic performance of the test piece.

Table 4. Characterized points of specimens.

Specimens	Yielding		Limit stage		Failure stage		Ductility Coefficient
	F_y, kN	Δ_y, mm	F_m, kN	Δ_m, mm	F_u, kN	Δ_u, mm	
FARC1	118.12	15.1	138.0	45.3	119.68	75.65	5.01
FARC2	122	15.3	148.2	45.9	124.27	80.1	5.24
FARC3	129	15.9	155	47.7	131.75	88.7	5.65
FARC4	125	15.5	150	46.5	127.5	80.6	5.20
ARC1	63.79	9.25	74.8	19.12	63.56	36.73	3.97
ARC2	67.63	9.43	79.8	19.71	68.20	39.10	4.15
ARC3	69.44	9.64	82.3	19.94	69.90	42.80	4.44
ARC4	68.87	9.55	80.6	19.84	68.52	39.25	4.11

The ductility coefficient of each specimen is calculated according to Eq. (1).

$$u = \frac{\Delta_u}{\Delta_y} \tag{1}$$

Where u is ductility coefficient.

The ductility coefficients of each test piece are presented in Table 4. It can be observed that the ductility coefficient of the test pieces FARC1 to FARC4 are significantly higher than that of the test pieces ARC1 to ARC4, which are increased by 26.17%, 26.26%, 27.25% and 26.52%, respectively. The main reason is that after the test piece yields, the outer square steel tube transforms the internal concrete damage from brittle failure to plastic failure, and optimizes the mechanical properties of the internal core concrete, thereby reducing the degree of decline in the bearing capacity of the test piece. Moreover, with the same Aeolian sand replacement rate, the outer square steel pipe exhibits better deformation-recovery ability, which is conducive to post–earthquake repair of specimens.

4. RESTORING FORCE MODEL

4.1 Skeleton Curve Model

Based on the experimental analysis, it can be stated that, with the presented method, the recovery force model established by Zhang Xianggang through steel tube recycled concrete frame [10], has been improved, and a three-fold line recovery force model that is suitable for square steel tube columns filled with Aeolian sand concrete is established. The skeleton of each specimen is mainly divided into three stages: elasticity, strengthening and ultimate failure. Therefore, the skeleton curve of the specimen is simplified into a trifold-line skeleton curve, whose theoretical model is shown in Fig. 4. The simplified skeleton curve uses dimensionless coordinates. A and A' are the positive and negative relative yield points of the specimen, respectively. Similarly, B and B' indicate the positive and negative relative peak points of the specimen. Meanwhile, the positive and negative relative failure points of the specimen are represented by C and C', respectively.

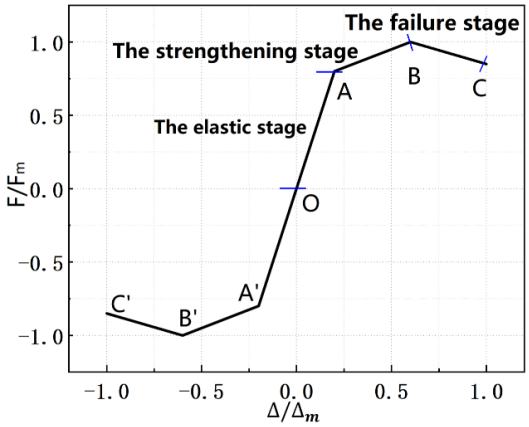

Fig. 4. Theoretical model of skeleton curve.

The linear equations of the OA, AB and BC segments of the skeleton curve theoretical model can be expressed as Eqs. (2-4).

$$\frac{F}{F_m} = 2.801\,1\frac{\Delta}{\Delta_m} \tag{2}$$

$$\frac{F}{F_m} = 0.780\,2\ + 0.229\,9\frac{\Delta}{\Delta_m} \tag{3}$$

$$\frac{F}{F_m} = 1.228\,9 - 0.225\,5\ \frac{\Delta}{\Delta_m} \tag{4}$$

The linear equations of the skeleton curve theoretical model OA', A'B' and B'C' are shown as Eqs. (5-7).

$$\frac{F}{|F_m|} = 2.813\,2\frac{\Delta}{|\Delta_m|} \tag{5}$$

$$\frac{F}{|F_m|} = -0.790\,6 + 0.217\,2\frac{\Delta}{|\Delta_m|} \tag{6}$$

$$\frac{F}{|F_m|} = -1.221\,8 - 0.234\,3\frac{\Delta}{|\Delta_m|} \tag{7}$$

The linear equation is used to analyze the theoretical model of the skeleton curve and the actual measured model. As shown in Fig. 5. T represents the measured skeleton curve, and M represents the theoretical skeleton curve. The theoretical model of the skeleton curve is in good agreement with the experimental measurement model. The result indicates that the theoretical model fitted by mathematical statistics can

better predict the skeleton curves of the specimens FARC1 to FARC4 under reversed cyclic loading.

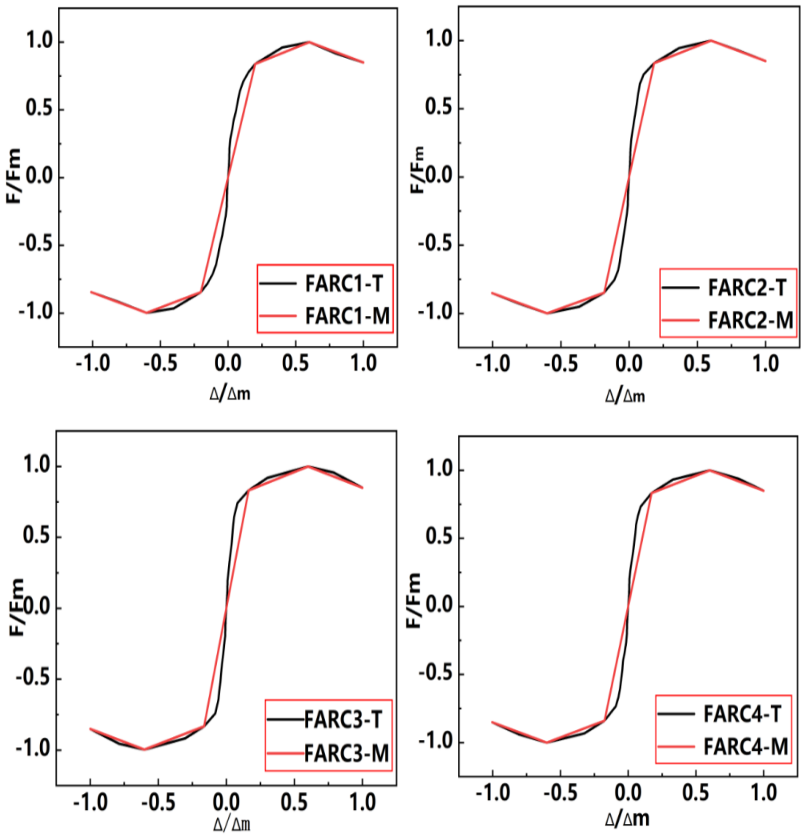

Fig .5. Test skeleton curve compared with the theoretical skeleton curve.

4.2 Law of Stiffness Degradation

The stiffness of loading and unloading under reversed cyclic loading gradually degrades as shown in Fig. 6. K represents the forward unloading stiffness, that is, the slope of the line connecting points 1 and 2; K' represents the negative unloading stiffness, that is, the slope of the line connecting points 3 and 4. Linear regression analysis is performed on the data of each specimen to obtain the unloading stiffness K and K' in the positive and negative directions. K_0 is the slope of the line connection between the origin and the yield point obtained through mathematical statistics of the measured data, that is, the initial stiffness of the test piece. A dimensionless analysis of the positive and negative unloading stiffness and lateral displacement of the specimens is conducted, as shown in Fig. 7. A good exponential function relationship appears

through fitting K/K_0 —Δ/Δ_m and K'/K_0 —Δ/Δ_m .The least squares method is used to fit and analyse the data, whose mathematical equation are Eqs. (8-9).

$$y = \beta e^{-x/b} + c \tag{8}$$

$$\beta = d - fa - ga^2 \tag{9}$$

Here, during forward loading, $y = K/K_0$, $x = \Delta/\Delta_m$, and when negative loading, $y = K'/K_0$, $x = \Delta/|\Delta_m|$. β is the correction coefficient and is related to the replacement rate of Aeolian sand a. By fitting the measured data of the test piece, b = *0.259 9*, c = *0.157 2*, and R^2=*0.985 9* under forward loading. For negative loading, b = *0.217 8*, c = *0.187 2*, and R^2=*0.941 9*. Therefore, the regression equations for the unloading stiffness in the positive and negative directions are Eqs. (10-12).

$$\frac{K}{K_0} = \beta e^{-\frac{\Delta}{\Delta_m}\cdot\frac{1}{0.259\,9}} + 0.157\,2 \tag{10}$$

$$\frac{K'}{K_0} = \beta e^{-\frac{\Delta}{|\Delta_m|}\cdot\frac{1}{0.217\,8}} + 0.187\,2 \tag{11}$$

$$\beta = 59.7577 - 150.0774a - 94.3743a^2 \tag{12}$$

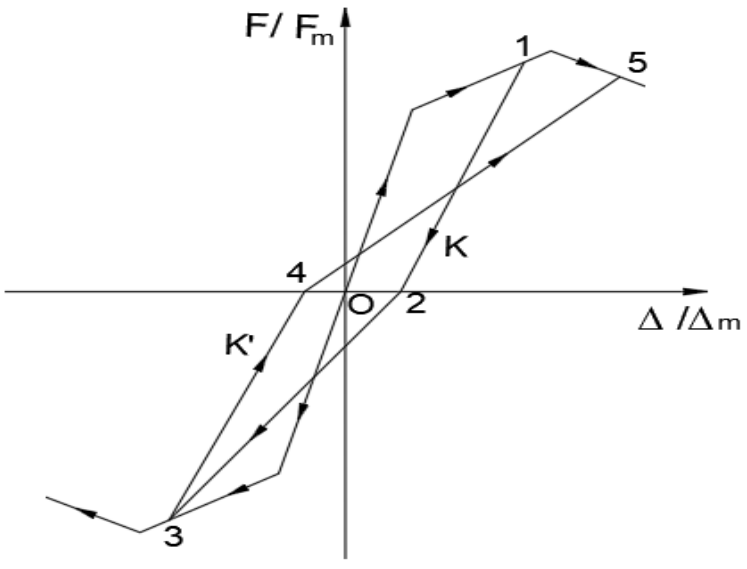

Fig. 6. Stiffness degradation rules**.**

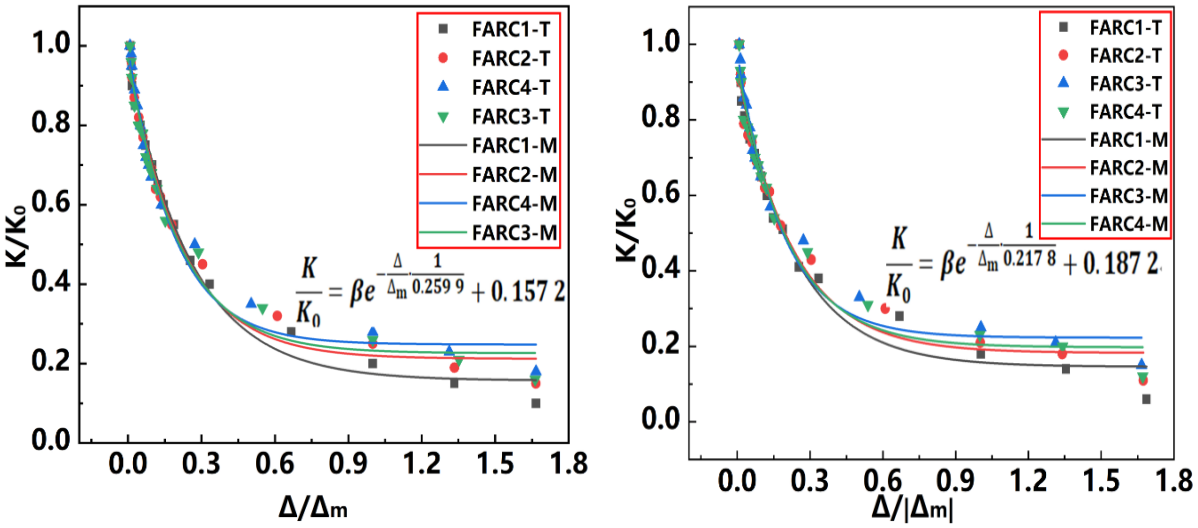

Fig. 7. Deterioration law of positive and negative stiffness.

4.3 Restoring Force Model

By combining the measured hysteresis curve of the test piece, the theoretical model of the skeleton curve, and the law of stiffness degradation, a method of treating the sudden drop in the bearing capacity of the displacement amplitude is used to establish a restoring force model suitable for square steel tube column filled with Aeolian sand concrete. The test specimens are conducted along the skeleton curve OABC (or OA'B'C') under reversed cyclic load, as shown in Fig. 8. The hysteresis rule can be stated as follows:

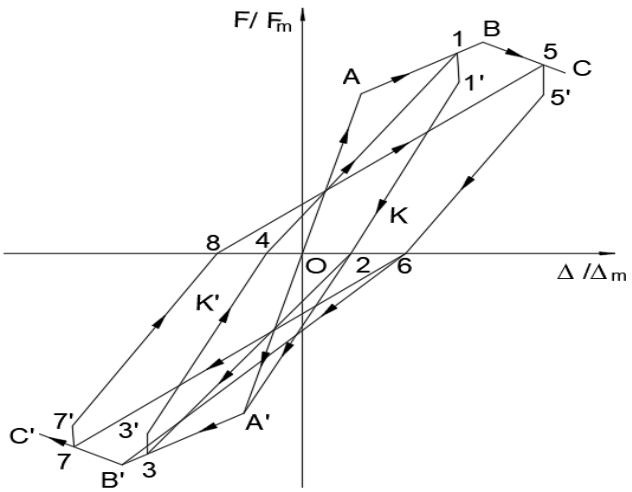

Fig. 8. Restoring force model.

1. According to the mathematical statistics of the measured data, the bearing capacity of the specimen immediately drops when the maximum displacement of each stage of positive and negative loading is reached and the specimen is unloaded after yielding. For the positive and negative loads after the sudden drop, it is suggested to take $0.7F_m$ and -$0.7|F'_m|$, respectively.
2. When the lateral load does not exceed the yield load F_y, the specimen is in the elastic stage, and the loading and unloading stiffness is approximately the initial test stiffness K_0 of the specimen. When loading in the OA (OA') section, the loading points to the positive (negative) relative yield point, and the unloading route proceeds along AO (A'O). When the AB section is unloaded, the bearing capacity first dropped to $0.7F_m$ (1' point) and unloaded along the path 1'2. The unloading stiffness is calculated by K. When the positive load is unloaded to zero (2 points) and then loaded in the negative direction, if the specimen is not yielded in that direction, it will point to the point A' and goes along the path 2A'B'C'. If the negative direction has yielded, it points to the maximum point 3 passed last time and goes along the path 23B'C'. When unloading at the A'B 'stage, the bearing capacity is first reduced to -$0.7|F_m|$ (point 3') and unloaded along the path 3'4. The unloading stiffness is calculated by K'. When the negative load is unloaded to zero (4 points) and loaded in the positive direction, it points to the maximum point 1 passed last time and goes along the 41BC path. When the specimen is unloaded at the BC in the failure stage, the horizontal bearing capacity is first reduced to $0.7F_m$ (5 'point) and unloaded along the path 5'6.The unloading stiffness is calculated according to K. Until unloading to zero (6 points) and loading in the negative direction, if the negative load of the specimen does not reach the peak load, it will point to the negative relative failure point B' and follow the path 6B'C'.If the negative load of the specimen exceeds the negative peak load, it points to the maximum point 7 passed last time and goes along the 67C' path. When B'C 'is unloaded in the specimen failure stage, the bearing capacity is first reduced to -0.7 $|F'_m|$ (7' point) and

unloaded along the path 7'8. The unloading stiffness is calculated according to K'. The negative load is unloaded to zero (8 points) and loaded in the positive direction, along the path 85C; and this trend continues in the same manner.

4.4 Comparison of Restoring Force Model and Test Results

The comparisons between the measured hysteretic curves of specimens and that of the restoring force model are shown in Fig. 9. Figure 9 shows that the measured model of each specimen is well with the theoretical model. Meanwhile, it can be stated that the modified restoring force model can well reflect the hysteretic relation between the load and the displacement.

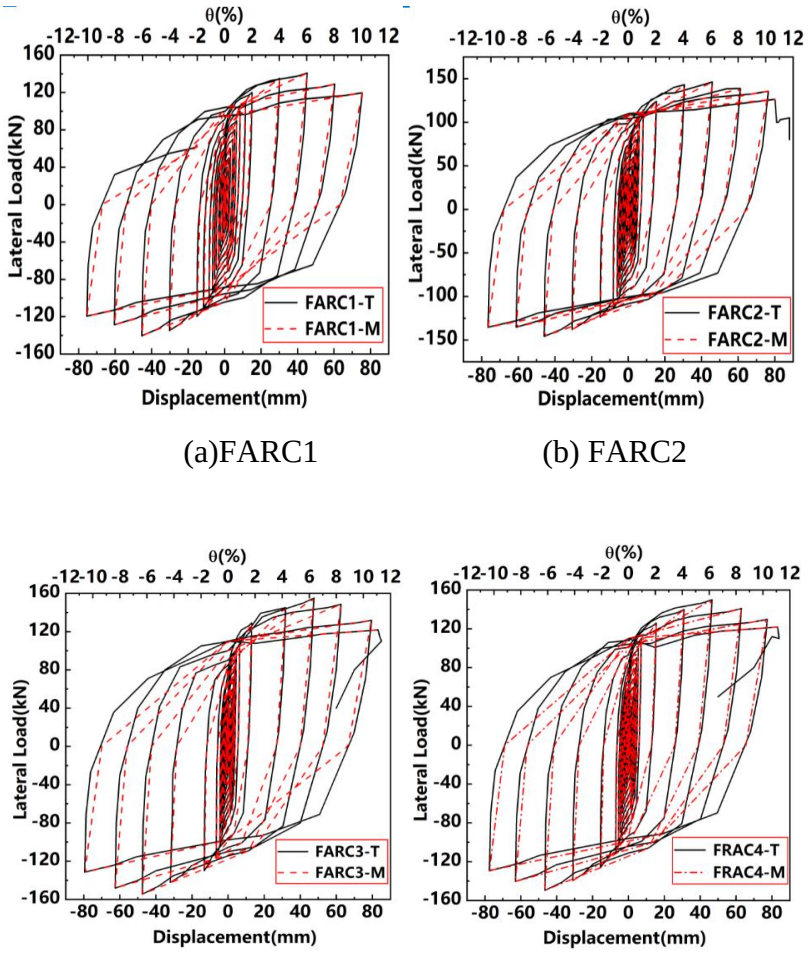

(a)FARC1 (b) FARC2

(c) FARC3 (d) FARC4

Fig. 9. Comparison of theoretical and experimental hysteresis curves.

5. CONCLUSIONS

This paper introduces the test results of four square steel tube columns filled with Aeolian sand concrete under reversed cyclic loads. By comparing and analysing the data of each specimen, the seismic damage process and the post-earthquake recovery force model were studied, and the following conclusions were drawn:

1. The hysteresis curves of the specimen FARC1 to FARC4 are relatively full and specimens FARC have good ductility, exhibiting good deformation capacity.
2. The results show that the hysteretic behavior, ductility and bearing capacity of the Aeolian sand concrete column can be effectively improved by installing an outside-square steel pipe. Therefore, the specimen FARC demonstrates better seismic behavior and post-earthquake recovery performance than the specimen ARC.
3. The restoring force model revised in this work conforms to the restoration process of the specimens in the test. Thus, it is practical and feasible to use this model to analyze the entire recovery process of square steel tube columns filled with Aeolian sand concrete.

DECLARATION OF CONFLICT OF INTERESTS

The authors have declared no conflict of interests.

ACKNOWLEDGMENTS

This paper was funded by the National Natural Science Foundation of China (51868059).

REFERENCES

1. Sonbul, A. R., Abu, S. E. S. S., and Hakami, B. A. H., “Experimental Study on the Utilization of Dune Sands as a Construction Material in the Area Between Jeddah and Mecca, Western Saudi Arabia”, Bulletin of Engineering Geology and the Environment, Vol. 75, No. 3, pp. 1007-1022, 2016.
2. Dong, W., Liu, S., and Xue, G., “Effect of Aeolian Sand and Fly Ash Content on Mechanical Properties of Concrete”, Bulletin of the Chinese Ceramic Society, Vol. 37, No. 7, pp. 2320-2325, 2018.

3. Dong, W., Shen, X. D., Xue, H. J., He, J., and Liu, Y., "Research on the Freeze-Thaw Cyclic Test and Damage Model of Aeolian Sand Lightweight Aggregate Concrete", Construction and Building Materials, Vol. 123, pp. 792-799, 2018.
4. Wu, C., Xu, S. C., Zhao, Q. S., and Yang, Y. K., "High Performance Concrete Filled Steel Tubular Short Column Seismic Performance Experimental Research", Industrial Construction, Vol. 49, No. 12, pp. 188-194, 2019.
5. Kotb, M. A., Ramadan, H. M., and Mourad, S. A., "Behavior of Rectangular Concrete Filled Steel Tubes Subjected To Torsion", Journal of Engineering and Applied Science, Vol. 62, No. 1, pp. 45-60, 2015.
6. Wang, J., Cheng, X. F., Yan, L. B., and Wu, C., "Numerical Study on I-section Steel-reinforced Concrete-Filled Steel Tubes (SRCFST) under Bending", Engineering Structures, Vol. 225, 2020.
7. Kenarangi, H., and Bruneau, M., "Shear Strength of Composite Circular Reinforced Concrete–Filled Steel Tubes", Journal of Structural Engineering, Vol. 146, No. 1, 2020.
8. Wang, G. Q., Li, Z. Q., Yang, S., and Ju, G. N., "Experimental Study of the Desert Sand Concrete Frame Columns under Low Cyclic Loading", Concrete, Vol. 6, No. 6, pp. 18–21, 2018.
9. Wang, Y. H., Chu, Q., and Han, Q., "Experimental Study on the Seismic Damage Behavior of Aeolian Sand Concrete Columns", Journal of Asian Architecture and Building Engineering, Vol. 19, No. 2, pp. 138-150, 2020.
10. Zhang, X. G., Chen, Z. P., and Xue, J. Y., "Research on the Restorative Force Model of the Recycled Concrete Steel Tube Frame", World Earthquake Engineering, Vol. 32, No. 1, pp. 277-283, 2016.